

In Situ Stress and Nanogravimetric Measurements During Hydrogen Adsorption/Absorption on Pd Overlayers Deposited onto (111)-Textured Au

G. R. Stafford* and U. Bertocci

Materials Science and Engineering Laboratory, National Institute of Standards and Technology, Gaithersburg, Maryland 20899

Received: March 17, 2009; Revised Manuscript Received: June 9, 2009

The stress induced by electrochemical hydrogen adsorption and absorption in very thin palladium layers electrodeposited onto (111)-textured gold has been examined in 0.1 M H₂SO₄ by the cantilever curvature method and by comparing resonant frequency changes on AT- and BT-cut quartz crystals. A compressive surface stress change of about -0.25 N m^{-1} is measured in the hydrogen adsorption region. Compressive stress for hydrogen adsorption is not expected from charge distribution models for adsorbate-induced surface stress but is consistent with first-principles calculations in the literature as well as experimental data for H adsorbed on Pt(111). Cantilever measurements in the hydrogen absorption region are consistent with a maximum atomic H/Pd loading of 0.63 and give a compressive stress-thickness change of -0.45 N m^{-1} per monolayer of Pd, corresponding to a biaxial stress change of -2.0 GPa . A somewhat lower value of -0.80 GPa for a H/Pd loading of 0.68 was obtained from EQNB data using the double crystal technique. These stress values fall well within the range of experimental values reported in the literature for β -hydride generated both electrochemically and from the gas phase.

Introduction

Epitaxially grown Pd overlayers on both Au (111) and Pt (111) have been used to study a wide variety of electrochemical phenomena such as hydrogen adsorption and absorption,^{1,2} formic acid and formaldehyde oxidation,^{3–5} carbon monoxide oxidation,⁶ and oxygen reduction.⁷ Pd deposition on Au(111) proceeds two-dimensionally in a layer-by-layer mode and grows pseudomorphically for at least the first few monolayers (MLs). Since the lattice mismatch between Pd and Au is +4.9%, the first few Pd layers have an expanded in-plane atomic spacing. Ruban has reported a d-band upward shift of 0.35 eV for a pseudomorphic Pd ML on Au(111).⁸ As a consequence, it has been argued that these laterally strained Pd adlayers can lead to fine-tuning of catalytic properties.⁵ Indeed, enhanced catalytic activity has been observed for Pd overlayers consisting of a few MLs.^{3,4,6} Recently we reported that the stress associated with the underpotential deposition (upd) of Pd on (111)-textured Au, as well as the growth of subsequent adlayers, is tensile, as expected from the lattice mismatch.⁹ The average biaxial film stress reaches a maximum value in adlayers that are two to three MLs thick. Interestingly this is the thickness regime that shows unique catalytic activity.

Ultrathin Pd overlayers on Au(111) are also useful substrates for studying hydrogen adsorption and absorption. Studying hydrogen adsorption on bulk Pd is challenging because the transient is dominated by the absorption process. It is therefore interesting to examine hydrogen adsorption on Pd thin films where the bulk absorption process can be limited, or, in the case of a Pd ML, completely eliminated. Several techniques have been used to produce high surface-to-volume Pd, including electrodeposition onto well-defined single crystals^{1,5,6,10,11} and a wide variety of polycrystalline substrates.^{12–15} Nanoscale Pd particles evaporated onto glassy carbon substrates have also been examined.¹⁶ The voltammetric response of these high surface/

volume Pd films clearly shows all of the potential dependent Pd-hydrogen interactions, including H adsorption, hydride formation (both α -Pd and β -Pd), and H₂ evolution. Pd adlayers electrodeposited onto a single crystal or highly textured substrates are particularly interesting because they allow us to examine these interactions as a function of adlayer thickness where the relative contributions can be varied.

An in situ probe gaining popularity in electrochemistry involves the measurement of surface and growth stress by monitoring the curvature of a wafer or cantilever while in solution and under potential control. Surface stress is the reversible work required to elastically deform a surface. Surface stresses arise because the atomic configuration of atoms at a surface is different than that in the bulk, the interior atoms exerting a stress on the surface atoms, i.e., the surface stress, that keeps them out of their equilibrium lattice positions. Changes in surface stress can provide information on surface reconstruction,^{17,18} adsorption processes,^{18,19} and thin film growth.^{20–22} Surface stress measurements on Pd overlayers of varying thickness would be particularly interesting since the stress contributions due to hydrogen adsorption and absorption can be distinguished and quantified.

Adsorbate induced surface stress is a topic of great interest to both the vacuum and electrochemical communities.^{19,23–27} Ibach has proposed a simple surface-induced charge redistribution model to explain the adsorbate-induced stress response.^{18,23} The local interaction of the adsorbate alters the bond strength between neighboring atoms on the surface. Electron donors would be expected to cause tensile stress since they increase the bond charge density between the underlying metal atoms whereas electron acceptors such as adsorbed anions cause compressive stress since they reduce the electron density in the surface. Hydrogen adsorption challenges this model. Hydrogen, being electropositive, is expected to induce a surface stress change in the tensile direction; however, compressive stress is observed experimentally on Pt(111) in both NaF²⁷ and HClO₄

* Corresponding author.

electrolyte.²⁴ Feibelman's first-principles calculations also show that H adsorption on Pt(111) relieves tensile stress, in spite of the fact that it produces a significant drop in the work function.²⁸ The surface stress change associated with hydrogen adsorption on Pd, without interference from hydrogen absorption, has yet to be reported.

The hydrogen absorption region has also been a topic of considerable interest and has been examined by several in situ techniques such as voltammetry,^{11,12,15} electrochemical quartz crystal nanogravimetry,^{29–33} piezoelectric response,³⁴ and wafer curvature.^{35–38} For the most part, the wafer curvature measurements have provided fundamental data on the hydride such as hydrogen diffusivity^{35,37} and stress state.^{38,39} Moreover, the curvature response of microcantilevers has also been exploited in the development of hydrogen sensors for the gas phase.^{40–43}

The palladium hydride equilibrium phase diagram at room temperature consists of a solid solution α phase (H/Pd \approx 0.03) and a NaCl-defect structure β phase (H/Pd \approx 0.6).⁴⁴ Several groups have generated the hydride electrochemically and report maximum H/Pd ratios ranging from 0.59 to 0.73.^{11,12,15,30,33} These studies also show that the $\alpha \rightarrow \beta$ transition occurs over a fairly narrow potential range, typically 20–50 mV. Since the lattice parameter of the β phase is 3.3% larger than that of the α phase, the $\alpha \rightarrow \beta$ transition causes a 10% volume expansion in the Pd. If the film is biaxially constrained, this volume expansion would give rise to a compressive stress on the order of -6.5 GPa. Stresses of such magnitude are likely not only to compromise the mechanical integrity of the film, but also its ability to absorb and store hydrogen.

In this paper, we examine the surface stress associated with the adsorption and absorption of hydrogen on ultrathin Pd overlayers electrodeposited onto (111)-textured Au cantilever electrodes. Making stress measurements on these Pd overlayers, which range in thickness from 1 to 9 ML, allows us to examine the surface stress change associated with first the adsorption and then the absorption of hydrogen on the Pd(111) surface, as a function of potential and Pd thickness. In a separate set of experiments, we examine the hydrogen region using an electrochemical quartz crystal nanobalance (EQNB) and show that a significant portion of the resonant frequency shift is stress induced, a phenomenon that has been widely reported in the literature.^{29–33} The stress generated in the palladium films due to hydride formation was calculated using the frequency shifts of both AT- and BT-cut crystals, according to the methods developed by EerNisse.^{29,45,46} The stress-corrected frequency shifts were then used to determine the mass change due to hydrogen absorption.

Experimental Section

In situ stress measurements were made on a HeNe optical bench using the wafer curvature method.^{22,47} The cantilever was a borosilicate glass strip (D 263, Schott) measuring 60 mm \times 3 mm \times 0.108 mm. Onto one side of the cantilever a 4 nm thick adhesion layer of titanium and a subsequent 250 nm film of gold were vapor-deposited by electron-beam evaporation at a temperature of 300 °C and growth rate of 0.1 nm s⁻¹. The Au electrodes had a strong (111) crystallographic orientation. The 200 reflection was not apparent in $\theta-2\theta$ X-ray scans and rocking curves of the 111 reflection generally yielded a full width half-maximum (fwhm) on the order of 2°. The curvature of the substrate was monitored while under potential control by reflecting a HeNe laser off of the glass/metal interface onto a position-sensitive detector. The relationship between the force per cantilever beam width, F_w , exerted by processes occurring

on the electrode surface and the radius of curvature of the cantilever, R , is given by Stoney's equation,⁴⁸

$$F_w = \frac{Y_s \cdot t_s^2}{6(1 - \nu_s)R} = \sigma t_f \quad (1)$$

where Y_s , ν_s , and t_s are Young's modulus, the Poisson ratio, and the thickness of the glass substrate, respectively. In the case where the force on the cantilever is due to surface processes, F_w is the surface stress. In the case where the force on the cantilever is the result of bulk processes, such as metal deposition or hydride formation, then F_w is equal to the stress-thickness product, i.e., the average biaxial film stress, σ , multiplied by the thickness of the film, t_f , as shown in eq 1. Since we measure curvature changes for both surface (adsorption) and bulk (absorption) processes, all curvature data will be presented as the stress-thickness product, σt_f . A more detailed description of the optical bench and stress measurement can be found in refs 22 and 47.

The electrochemical cell was a single-compartment Pyrex cell covered by a polytetrafluoroethylene cap. A glass disk was joined to the back of the cell to allow it to be held and positioned by a standard mirror mount on the optical bench. The counter electrode was a platinum foil placed parallel to and in the same solution as the working electrode. The reference electrode was a saturated Hg sulfate electrode (SSE) that was separated from the working compartment by a Vycor-tipped bridge filled with saturated K₂SO₄ solution. All potentials are referenced to the SSE. Prior to making a measurement, the electrolyte was purged with argon. Potential control was maintained using an EG&G Princeton Applied Research Corp. (PARC) model 273 potentiostat-galvanostat that was controlled by a Dell Pentium 4 computer and LabView software.

Prior to Pd deposition the (111)-textured Au cantilever electrode was cleaned in piranha solution (3:1 volume mixture of concentrated H₂SO₄:30% H₂O₂). The cantilever was then mounted in the cell and placed on the optical bench. The Pd adlayers were then electrodeposited from 0.1 mol L⁻¹ H₂SO₄ (Mallinckrodt) containing 1.0 mmol L⁻¹ H₂PdCl₄. The H₂PdCl₄ was formed by adding stoichiometric quantities of PdSO₄ and HCl (Fisher).⁴⁹ Deposition was controlled potentiostatically to a desired film thickness that was determined from the charge passed, based on a ML charge of 446 μ C cm⁻². This assumes that the Pd is pseudomorphic with the Au and deposits with a uniform current distribution. The stress-thickness was monitored during Pd deposition to ensure that each deposit had a growth stress signature appropriate for its thickness. Following Pd deposition, 18.3 M Ω cm distilled water was flushed through the cell in order to remove the Pd²⁺. The hydrogen adsorption/absorption experiments were then conducted in deaerated 0.1 mol L⁻¹ H₂SO₄, in the absence of Pd²⁺.

An EQNB (Maxtek, Inc.) was used to measure both the stress generation and mass changes during hydrogen absorption into the Pd adlayers. The quartz crystals (Maxtek, Inc.) were polished 2.54 cm AT-cut and BT-cut disks onto which first Ti and then Au was vacuum deposited. The fundamental resonance frequency was 5 MHz. The Au deposit had a strong (111) crystallographic orientation and rocking curves of the 111 reflection generally yielded a fwhm on the order of 3°. The Au had a roughness factor of 1.3, based on the charge necessary for the complete reduction of the Au oxide during potentiodynamic sweeps.⁵⁰ The EQNB as well as the EG&G 273 potentiostat-galvanostat were driven by Labview software on

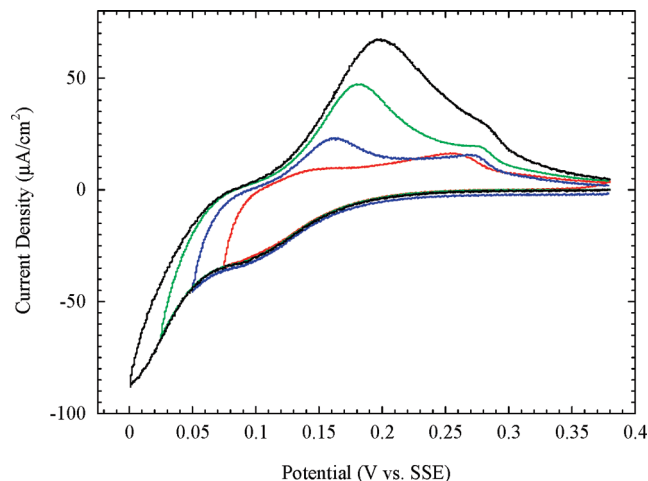


Figure 1. Potentiodynamic scans for (111)-textured Au in 0.1 mol L⁻¹ H₂SO₄ and 1.0 mmol L⁻¹ H₂PdCl₄. Variation of the cathodic vertex at constant sweep rate of 5 mV s⁻¹.

a Macintosh Power PC computer. The glass cell for the EQNB measurements had separate compartments for the working, counter, and SSE reference electrodes, the latter being connected via a Luggin–Haber capillary. The cell had a magnetic stirrer, and high purity Ar was either bubbled in the main compartment or swept above the solution to maintain a small overpressure inside the cell. The Pd adlayers were electrodeposited from 0.1 mol L⁻¹ H₂SO₄ containing 1.0 mmol L⁻¹ H₂PdCl₄. Deposition was controlled potentiostatically to a desired film thickness that was determined from the mass deposited, based on an ML mass of 350 ng/cm². Since we examine thicker films with the nanobalance, we assume that the Pd loses coherency with the Au and grows with the in-plane lattice spacing of bulk Pd. This ML mass also takes into account the 1.3 roughness factor.

Results

Figure 1 shows the voltammetry of the (111)-textured Au cantilever in 0.1 mol L⁻¹ H₂SO₄ containing 1.0 mmol L⁻¹ H₂PdCl₄ where the cathodic vertex is adjusted to more negative values so that both Pd upd and bulk deposition occur. The potential of zero charge (pzc) for Au(111) in this electrolyte is -0.19 V versus SSE,⁴⁹ so the Au has an adsorbed layer of [PdCl₄]²⁻ on the surface in the Pd upd region.^{49,51} It is believed that Pd deposition occurs by reductive discharge of the adsorbed Pd chloro complex. Pd upd begins at about 0.20 V, and the observed separation between upd and overpotential (opd) or bulk deposition occurs at 0.08 V. This potential range for Pd upd is identical to that reported by Baldauf.¹ It should be noted that the kinetics of the upd tends to be rather sluggish, and it is not always possible to separate upd from opd. Anodic stripping of the opd layer occurs at about 0.16 V, whereas the peak at about 0.27 V corresponds to the dissolution of the upd layer.

The earliest stages of Pd deposition on Au(111) have been examined by STM.^{1,51} At potentials positive of Pd²⁺ reduction, the Au surface is covered with an adlayer of [PdCl₄]²⁻. Pd upd begins at the monatomic steps and at the rims of the Au islands that appear on the surface due to lifting of the Au(111) reconstruction. Eventually the entire Au surface is covered with a ML of Pd, which cannot be atomically resolved due to the readsorption of [PdCl₄]²⁻ on the Pd surface. When the potential is adjusted to the opd region, a second Pd layer grows two-dimensionally, while a third layer starts before the second layer is finished. It has been reported that at least four MLs can be

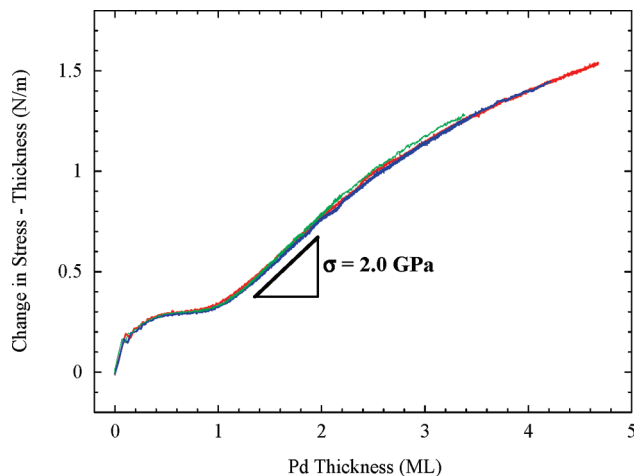


Figure 2. Stress-thickness product for potentiostatic deposition of Pd onto (111)-textured Au in 0.1 mol L⁻¹ H₂SO₄ containing 1.0 mmol L⁻¹ H₂PdCl₄. Nominal deposit thicknesses and deposition potentials are (red curve) 4.7 ML (0.05 V), (blue curve) 4.2 ML (0.06 V), and (green curve) 3.4 ML (0.07 V). Deposit thicknesses are based on a ML charge density of 446 μC cm⁻².

grown pseudomorphically on the Au. When the Pd is stripped at positive potentials, the Au(111) surface is identical to the initial state and there is no indication of surface alloying which has been reported for polycrystalline Au.^{49,52} EQNB examinations of the deposition process report mass/charge values of -0.53 ng μC⁻¹, quite close to the theoretical value of -0.55 ng μC⁻¹, assuming a 2e⁻ reduction to Pd metal.^{9,51} This *m/Q* value confirms that the adsorbed [PdCl₄]²⁻ is not desorbed but remains on the surface of the Pd ML so that the mass change is only due to the Pd.

Pd adlayers of varying thickness were electrodeposited potentiostatically onto the (111)-textured Au cantilever electrodes while the cantilever curvature was measured to reveal the changes in stress during growth. Figure 2 shows the stress-thickness product (σt_f in eq 1) for three separate films having nominal thicknesses between 3.4 and 4.7 ML that were electrodeposited at three different potentials in the opd region (0.05 V, 0.06 V, and 0.07 V). The upd and opd regions each have unique stress signatures, although both clearly are under tensile stress. The primary driver of the tensile stress is the +4.9% lattice mismatch between Pd and Au. Pd upd causes a stress-thickness change of +0.3 N m⁻¹, whereas the second ML produces an additional change of +0.45 N m⁻¹. We attribute this larger tensile stress change for the second ML to the diminished electronic influence of the Au substrate, which has a compressive contribution to the surface stress change.⁹ This +0.45 N m⁻¹ stress-thickness for the second ML corresponds to a biaxial stress of 2.0 GPa. This is about a factor of 7 less than one would calculate from a simple elasticity model using the difference between the bulk lattice parameters to determine a misfit strain.¹⁸ This lower than expected tensile stress may be due to the adsorption of [PdCl₄]²⁻, which can stabilize an expanded Pd structure, much the same way that sulfate has been reported to expand the surface atoms of Cu,^{53,54} thereby reducing the coherency strain of the Cu ML on Au(111).²⁵ It is also clear from these measurements that the tensile stress is not linear but decreases as the film thickens, suggesting that the Pd begins to lose coherency with the Au substrate. This appears to contradict STM evidence that the first four MLs of Pd grow pseudomorphically with the Au(111) surface.⁴⁹

We now examine these Pd adlayers for hydrogen uptake in acid. As mentioned previously, the hydrogen adsorption reaction

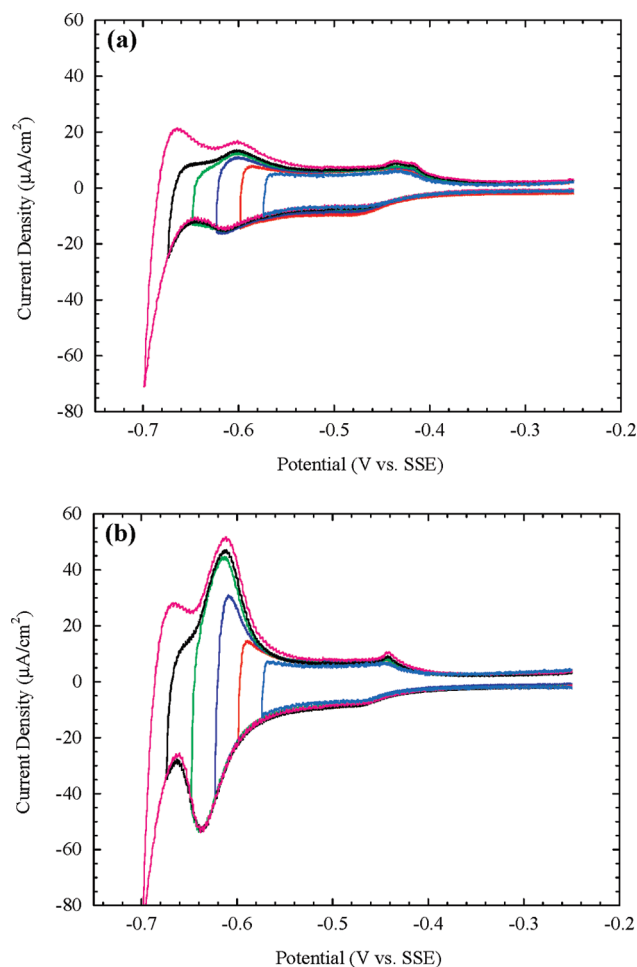


Figure 3. Potentiodynamic scans (5 mV s^{-1}) in the hydrogen region for (a) 3 MLs and (b) 6 MLs of Pd in $0.1 \text{ mol L}^{-1} \text{ H}_2\text{SO}_4$. The Pd films were electrodeposited onto (111)-textured Au from $0.1 \text{ mol L}^{-1} \text{ H}_2\text{SO}_4$ containing $1.0 \text{ mmol L}^{-1} \text{ H}_2\text{PdCl}_4$.

is difficult to study on bulk Pd because it is masked by the hydrogen absorption reaction. This can be circumvented by using thin Pd overlayers rather than bulk material. Figure 3 shows voltammetry in the hydrogen region for Pd adlayers that are nominally 3 and 6 ML. Hydrogen adsorption begins at about -0.45 V , whereas hydrogen absorption occurs between -0.56 and -0.66 V . This is followed by hydrogen evolution at more cathodic potentials. The primary difference in the voltammetry for 3 and 6 ML adlayers is the amount of charge associated with hydrogen absorption. As expected, the hydrogen adsorption and H_2 evolution transients are similar for the two adlayer thicknesses since these processes are confined to the surface. An additional yet subtle difference between the two curves involves the anodic peak at -0.44 V , which is attributed to hydrogen desorption/sulfate adsorption.^{1,5} Kibler has shown a thickness dependence on the peak potential, noting that the peak for a Pd ML is located about 30 mV more positive than that for single crystal Pd.⁵ The 2 ML adlayer shows a doublet for the H desorption, one corresponding to the ML while the other corresponds to the single crystal. Similar behavior is shown in Figure 3. The hydrogen desorption region for the 3 ML adlayer consists of two peaks, whereas only the more negative of the two peaks is observed for the 6 ML adlayer. This nicely demonstrates the transition between desorption from a strained adlayer and that from a surface behaving more like bulk Pd. This 30 mV difference in hydrogen desorption potential is similar to the shift in the pzc for similarly thick Pd films.⁵⁵

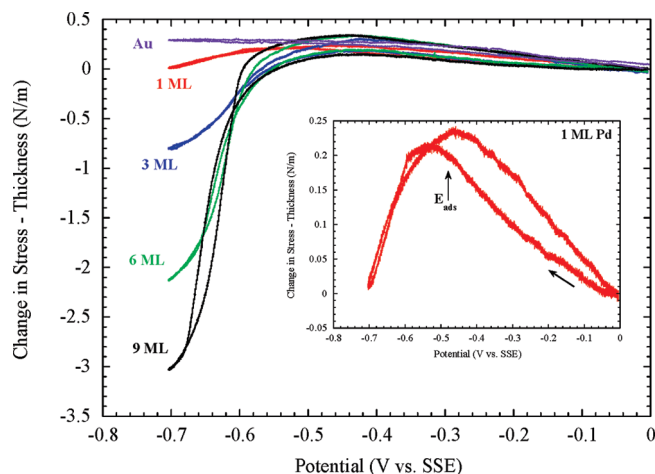


Figure 4. Stress-thickness response to potentiodynamic scans shown in Figure 3 for 1, 3, 6, and 9 MLs of Pd electrodeposited onto (111)-textured Au. The response of a (111)-textured Au cantilever is also shown for comparison. The inset shows the magnified response for the 1 ML Pd cantilever electrode.

Figure 4 shows the stress-thickness response for Pd adlayers of varying thickness in the potential region shown in the Figure 3 voltammetry. The stress response for a single ML of Pd is shown in the inset in order to better resolve the response. The stress curves show that the surface stress moves in the tensile (positive) direction from a value arbitrarily chosen as zero at 0.0 V , the starting potential. The pzc for Pd(111) is reported to be -0.535 V/SSE in dilute NaF^{55} and -0.55 V/SSE in $0.05 \text{ M Na}_2\text{SO}_4$ acidified to a pH of 3.⁵⁶ As a consequence, an increase in surface stress in the potential region of 0 to -0.4 V would be expected due to electrocapillarity, with some additional contribution due to sulfate desorption from the Pd surface. The stress-thickness response for the Pd adlayers begins to deviate from that of the bare Au surface at a potential of about -0.52 V , just negative of the hydrogen adsorption potential on Pd. A compressive stress of about -0.25 N m^{-1} is associated with hydrogen adsorption. This is clearly seen in the inset for the 1 ML Pd adlayer where hydrogen absorption cannot occur. The compressive stress response for H adsorption is contrary to charge distribution models for adsorbate-induced surface stress¹⁸ but supports first-principles calculations²⁸ as well as experimental data^{24,27} for H on Pt(111). The asymmetry in the stress-thickness response for hydrogen adsorption and desorption (inset) has also been observed in the electrochemical transients for hydrogen adsorbed onto Pd adlayers grown on Au(111) single crystal.¹ This has been attributed to a two-dimensional nucleation and growth process for the formation of the hydrogen adlayer, the kinetics of which is controlled by sulfate desorption/adsorption.

Figure 4 also shows that the absorption of H into the Pd adlayer results in a significant compressive stress-thickness product. Further, the magnitude of the stress-thickness change increases with increasing Pd adlayer thickness. When the potential scan is reversed, the stress-thickness essentially duplicates the cathodic transient. The shape of the stress-thickness–potential curves is very similar to the H/Pd capacity–potential curves reported in the literature.^{11,12,15,30,32,33} As mentioned previously, hydride formation begins with the formation of the solid solution α phase ($\text{H/Pd} \approx 0.03$), which eventually converts to the β phase ($\text{H/Pd} \approx 0.6$).⁴⁴ Over a fairly narrow potential region, there exists a two-phase region where only the relative amounts of each phase change. This two-phase region is typically centered in the potential range of -0.63 to

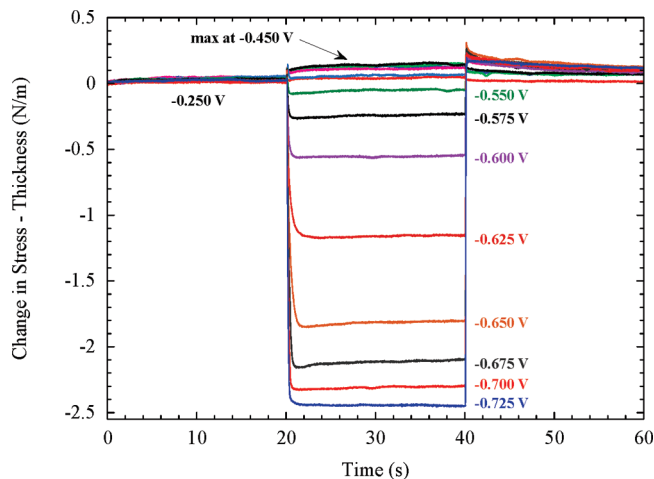


Figure 5. Stress-thickness response to cathodic potential steps from a starting potential of -0.250 V vs SSE in $0.1 \text{ mol L}^{-1} \text{ H}_2\text{SO}_4$ for 6 ML of Pd electrodeposited onto (111)-textured Au.

-0.67 V/SSE .^{11,12,15,30,32,33} Since stress generation is due to the volume expansion associated with the $\alpha \rightarrow \beta$ transition, then the stress transient should coincide with the two-phase region and the potential window cited above. Once the β -phase is fully formed, the stress-thickness should reach a constant value and scale with the Pd adlayer thickness. This is the behavior observed in Figure 4.

An excellent way to further examine the stress response is through a series of potential pulses into the hydrogen adsorption/absorption region. Figure 5 shows the stress-thickness response of a 6 ML Pd film to a series of 20 s pulses from a starting potential of -0.25 V. In all cases, the stress-thickness responds fairly quickly to the potential step, stabilizing to a steady state value within a few seconds. When the cantilever electrode is pulsed to a potential positive of hydrogen adsorption (-0.45 V), the stress-thickness response is slightly tensile, reflecting both electrocapillarity and the desorption of sulfate. The tensile stress reaches its maximum value following the step to -0.45 V. At more negative potentials, the stress response is less tensile and becomes net compressive at -0.55 V, reflecting the adsorption of hydrogen. At more negative potentials, hydrogen absorption begins and significant compressive stresses are observed. Even in the Pd absorption region, the stress-thickness response is only a function of potential, not time, since the absorption kinetics are rapid and the adlayers are quite thin. In addition, the potential dependence is a clear indication that the hydrogen absorbed in the Pd adlayer is in thermodynamic equilibrium with the hydrogen activity at the surface. Upon reversing the potential back to a value of -0.25 V, the cantilever returns to its original position, although this may take several seconds.

Figure 6 shows a plot of the stress-thickness change, taken as the average of the cathodic and anodic stress response (Figure 5), as a function of the step potential, for Pd adlayers of varying thickness. The general shape of the curves is essentially identical to that measured during the potentiodynamic scans shown in Figure 4. The stress-thickness becomes mildly compressive in the hydrogen adsorption region, -0.50 V, and significantly compressive and thickness dependent once hydrogen absorption begins at about -0.55 V.

In an attempt to determine the quantity of hydrogen absorbed into the various Pd adlayers, the voltammetry in Figure 3 was integrated in the potential range between hydrogen adsorption and H_2 evolution. It should be noted that anodic stripping

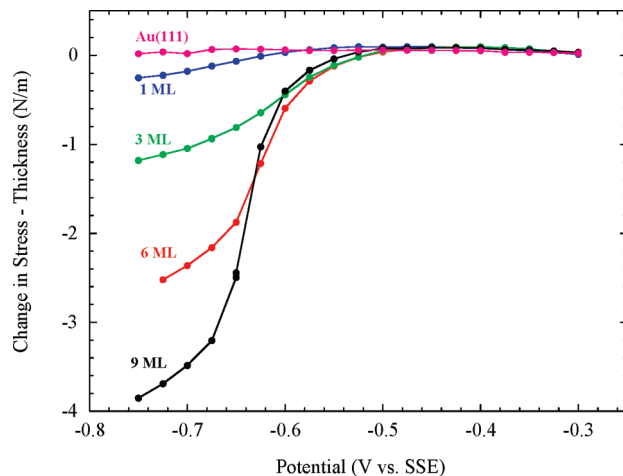


Figure 6. Plot of average stress-thickness change versus step potential in $0.1 \text{ mol L}^{-1} \text{ H}_2\text{SO}_4$ for 1, 3, 6, and 9 MLs of Pd electrodeposited onto (111)-textured Au. The response of a (111)-textured Au cantilever is also shown for comparison.

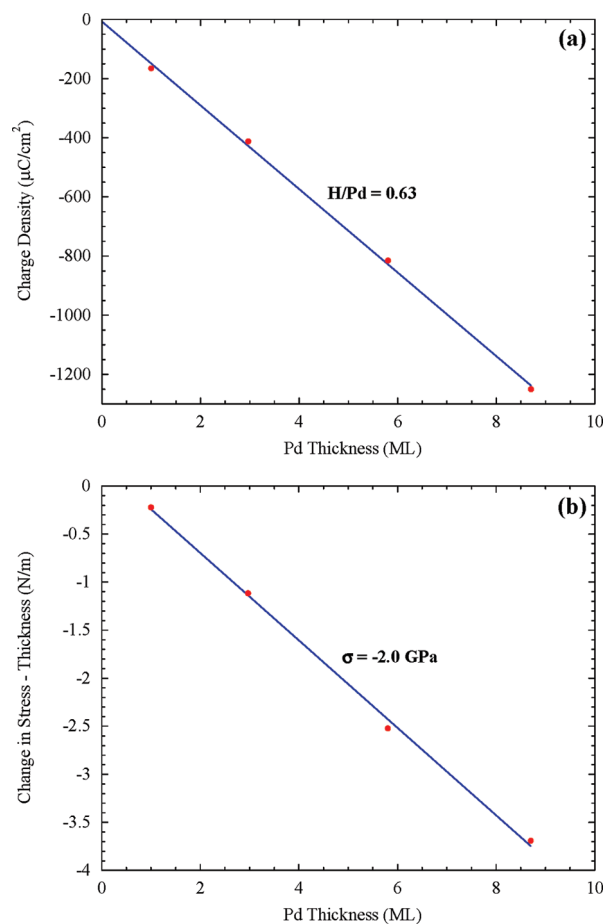


Figure 7. (a) Plot of charge density for hydrogen adsorption/absorption versus Pd deposit thickness. The charge density was obtained by integrating the current from potentiodynamic scans similar to those shown in Figure 3. (b) Change in stress-thickness for hydrogen adsorption/absorption versus Pd deposit thickness (from Figure 6 data).

voltammetry following a potentiostatic hold is a more accurate method for measuring hydrogen capacity and has been used by several research groups to generate reproducible capacity-potential curves.^{11,12,15,30,32,33} Figure 7a shows a plot of the total charge as a function of the Pd adlayer thickness, in MLs. The plot is a straight line that intersects the origin. The slope of the line

was used to calculate an average capacity of 0.63 H atoms per Pd atom in the adlayer. This is close to the 0.6 H/Pd room temperature capacity reported for the β phase from the equilibrium phase diagram⁴⁴ as well as experimental values for electrochemical hydrogen absorption.^{11,12,15,30,32,33} The charge density measured for the 1 ML Pd deposit is $150 \mu\text{C cm}^{-2}$, which is less than the expected $223 \mu\text{C cm}^{-2}$ for a hydrogen ML. However, this lower value is consistent with reports in the literature for hydrogen adsorption on a upd layer of Pd on Au(111).¹

In addition to the capacity–thickness plot shown in Figure 7a, a similar stress–thickness–Pd–thickness plot was constructed from the average stress–thickness change measured for the -0.725 V pulse shown in Figure 6. Figure 7b shows that the average stress–thickness change also increases linearly with the Pd adlayer thickness. An average biaxial stress of -2.0 GPa can be calculated for the β -Pd hydride from the slope of the line, after converting the Pd thickness from MLs to nanometers. This is about a factor of 5 less than the -9.6 GPa expected for the reported 10% volume expansion for the fully charged β -Pd (H/Pd = 0.6) using

$$\sigma = -\frac{E_{111}}{1 - \nu_{111}} \frac{\Delta V}{3V} \quad (2)$$

where E_{111} is Young's modulus of Pd, ν_{111} is Poisson ratio, and $\Delta V/V$ is the volumetric strain due to the expansion. Since the Pd adlayers have a (111) crystallographic orientation, the (111) single crystal values of the modulus (136.5 GPa) and Poisson ratio (0.53) obtained from the elastic compliances⁵⁷ are used.

The -9.6 GPa residual stress calculated above assumes that the $\alpha \rightarrow \beta$ transition requires a 10% volume expansion in the Pd while the film is biaxially constrained. Here we consider the possible influence of the expanded Pd structure, assuming coherency with the underlying Au surface. Figure 2 confirms that these layers are under a tensile stress; i.e., a negative stress-free strain. The lattice is expanded, and a negative strain is required to alleviate the tensile stress. If the Pd is coherent with respect to the Au surface, then the stress free strain is -0.049 , based on the bulk lattice parameters of Au and Pd, [$\epsilon_{sf} = -(a_{Au} - a_{Pd})/a_{Pd}$]. However, once the Pd is converted to the β hydride the stress free strain is reduced to -0.014 , based on the bulk lattice parameters of Au and β -Pd and assuming the Pd continues to occupy the 3-fold site of the Au. The curvature of the cantilever would respond to the reduction in the stress free strain and produce a stress change in the compressive direction. Although the stress state of the Pd prior to charging might influence the charge capacity, the stress free strain argument above suggests that it will not alter the magnitude of the stress change, only the final value of the residual stress. For example, Figure 2 shows that a 5 ML adlayer of Pd causes a $+1.6 \text{ N m}^{-1}$ change in the stress-thickness. The same adlayer, when converted to β -Pd, undergoes a -2.2 N m^{-1} stress-thickness change (Figure 7b). The net stress-thickness on the Pd is about -0.6 N m^{-1} (-0.5 GPa). If, on the other hand, the 5 ML of Pd were not epitaxial on Au, but managed to deposit stress free, the stress-thickness change upon hydride formation (assuming equal capacity) would still be -2.2 N m^{-1} ; however, this film would have a residual stress-thickness of -2.2 N m^{-1} (-2.0 GPa). Although the overall stress change is directly proportional to the amount of hydrogen in the Pd, lattice matching the Pd to establish a tensile stress prior to charging reduces the residual compressive stress once the hydride is formed.

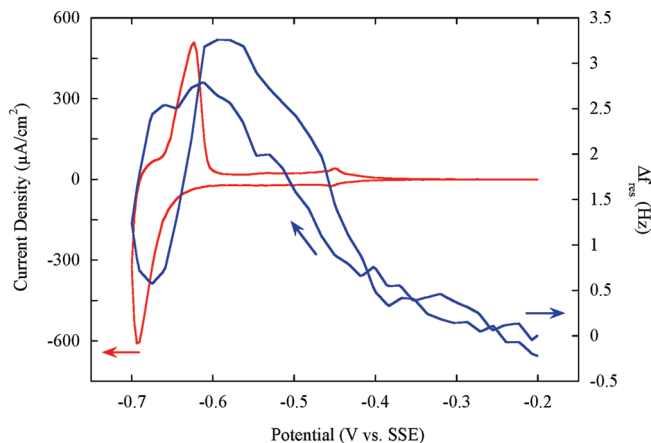


Figure 8. Potentiodynamic scan and mass change for 15 ML thick Pd deposit on (111)-textured Au in $0.1 \text{ mol L}^{-1} \text{ H}_2\text{SO}_4$. Sweep rate = 10 mV s^{-1} .

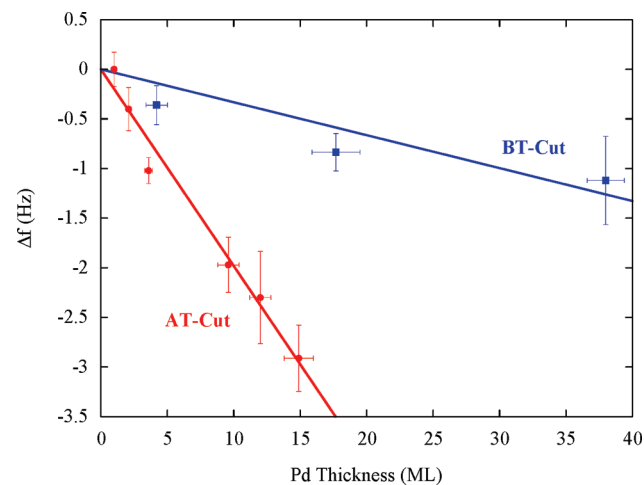


Figure 9. Plot of frequency shift due to hydrogen absorption in Pd adlayers of varying thickness, deposited onto AT- and BT-cut quartz crystals. The frequency shift was measured prior to the onset of hydrogen evolution during 5 mV s^{-1} potentiodynamic scans.

The adsorption and absorption of hydrogen on thin electrodeposited Pd was also examined with the EQNB. A typical frequency response on an AT-cut crystal during a potentiodynamic scan is shown in Figure 8. The mass signature for a hydrogen ML is too small for reliable detection, particularly since hydrogen adsorption and sulfate desorption occur simultaneously. The observed increase in frequency in the hydrogen adsorption region is due to sulfate desorption. In contrast, a considerable decrease in the resonant frequency is observed in the hydrogen absorption region. It has been recognized for some time that a significant portion of the resonant frequency shift is stress induced.^{29,33,45,46} However, an interesting feature is that the stress/frequency shift characteristics are dependent on the crystallographic orientation of the quartz crystal. The effect of the stress on the frequency response of an AT-cut crystal is the opposite of that on a BT-cut crystal. This allows one to differentiate the stress and mass contributions to the resonant frequency shift by making identical measurements using two crystals of different orientation. Figure 9 shows the frequency shift for both AT-cut and BT-cut crystals as a function of the Pd thickness following potentiodynamic scans into the hydrogen absorption region. Both data sets can be fit to a straight line passing through the origin. The slope of the two curves yields the frequency response per ML of Pd for the AT-cut crystal, $\Delta f_{\text{ML}}^{\text{AT}}$, to be $-0.198 \pm 0.045 \text{ Hz ML}^{-1}$ and for the BT-cut

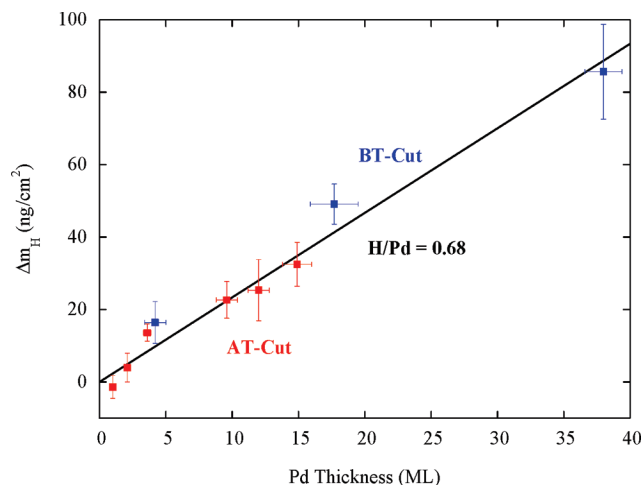


Figure 10. Mass increase due to hydrogen absorption in Pd adlayers of varying thickness, obtained from frequency shift that was corrected for stress using AT- and BT-cut quartz crystals.

crystal, $\Delta f_{\text{ML}}^{\text{BT}}$, to be $-0.033 \pm 0.011 \text{ Hz ML}^{-1}$. The stress-thickness product of the Pd adlayer, σt_f , can be quantified using the method of EerNisse,^{29,45,46}

$$\sigma t_f = \frac{1}{K^{\text{AT}} - K^{\text{BT}}} \left[t_q^{\text{AT}} \frac{\Delta f_{\text{ML}}^{\text{AT}}}{f_{\text{res}}^{\text{AT}}} - t_q^{\text{BT}} \frac{\Delta f_{\text{ML}}^{\text{BT}}}{f_{\text{res}}^{\text{BT}}} \right] \quad (3)$$

where K is the stress coefficient, t_q is the thickness of the quartz crystal, Δf_{ML} is the frequency shift, and f_{res} is the fundamental resonant frequency, for each of the crystal types. The stress coefficients K^{AT} and K^{BT} have the values $2.75 \times 10^{-11} \text{ m}^2 \text{ N}^{-1}$ and $-2.65 \times 10^{-11} \text{ m}^2 \text{ N}^{-1}$, respectively. The quartz crystal thicknesses are 0.033 and 0.0508 cm respectively for AT- and BT-cut crystals. The fundamental resonant frequency of both crystals is 5 MHz. Using the frequency shifts obtained from the slopes of the curves in Figure 9, one can calculate a σt_f per ML of Pd of $-0.180 \pm 0.043 \text{ N m}^{-1}$. An average biaxial stress in the Pd adlayers of $-0.80 \pm 0.20 \text{ GPa}$ is obtained by dividing σt_f by the thickness of the Pd ML, or 0.224 nm. It should be noted here that, although we chose to normalize σt_f per ML of Pd, the frequency response data was averaged from adlayers up to 40 ML in thickness. As a consequence, the biaxial stress of -0.80 GPa calculated from the EQNB data is representative of Pd adlayers up to at least 40 ML thick.

The stress-thickness product, σt_f , can be used to remove the stress component of the frequency shifts in order to determine the mass change due to hydrogen absorption. The effect of stress on the resonant frequency of the quartz crystal, Δf_s , is expressed by the relationship

$$\Delta f_s^{\text{AT}} = \frac{f_{\text{res}}^{\text{AT}} K^{\text{AT}} \sigma t_f}{t_q^{\text{AT}}}, \quad \Delta f_s^{\text{BT}} = \frac{f_{\text{res}}^{\text{BT}} K^{\text{BT}} \sigma t_f}{t_q^{\text{BT}}} \quad (4)$$

where the terms have been defined above and are specific to a particular crystal cut. These adjustments were applied to the data in Figure 9, and the corrected frequency shifts were converted to mass using the Sauerbrey equation.^{58,59} Figure 10 shows the results plotted as a function of the Pd adlayer thickness. The data from both crystals can be fit to a single straight line with a slope of $2.33 \text{ ng cm}^{-2} \text{ ML}^{-1}$ of Pd. This is equivalent to a hydrogen loading of 0.68 H/Pd, slightly higher

than the hydrogen capacity measured from the cantilever voltammetry, yet well within the range of saturation values quoted in the literature.

Several research groups have measured the stress associated with Pd hydride formation. The most direct method is based on wafer curvature measurements as reported here. Sahu measured the curvature during the galvanostatic charging of 0.1 μm Pd films that were sputtered onto glass cantilevers and reports stress-charge values of -1.29 N C^{-1} for loadings less than H/Pd = 0.04, at which point the Pd delaminated from the glass.³⁸ Assuming this stress-charge relationship is linear for higher H loading, a stress of -8.4 GPa is expected for a H/Pd of 0.6. Similar measurements have been made during hydride formation from the gas phase on Pd cantilevers of similar geometry. Curvature values which convert to a compressive stress of about -2.5 GPa have been reported at H_2 pressures of 100 Torr (13.3 kPa), corresponding to a H/Pd = 0.45.³⁹ Stress values have also been estimated from single-cut EQNB data, where the mass-induced frequency shift is estimated from the charge, and the EerNisse treatment^{45,46} is then applied to the modified resonant frequency shift to determine the stress. Stress values for β -Pd hydride ranging from -2.0 to -4.5 GPa have been reported.^{31,33} Cheek and O'Grady, using the double crystal method reported here, measured a compressive stress of -1.0 GPa in a fully charged 400 nm thick Pd film.²⁹

The stress changes reported here, for hydrogen absorption into ultrathin Pd adlayers, are on par with experimental values reported in the literature for much thicker films of β -hydride formed both electrochemically and from the gas phase. It is interesting to note that, although the stress value we obtain from the double crystal EQNB technique is about half of that measured by our cantilever beam, it is very close to the -1.0 GPa value for 400 nm Pd films reported by Cheek and O'Grady using the same double crystal method used here.²⁹ Although we do not fully understand the reason for the discrepancy, we note a couple of items regarding the EQNB data. The first is the large error bars associated with the frequency data (Figure 9) and the generally poor linear fit of the BT-cut crystal data. Our propagation of error analysis indicates that there is a 25% uncertainty in the average film stress obtained from this data. The second is the fact that the cantilever data was restricted to Pd thicknesses of less than 10 ML whereas the EQNB data was obtained from films up to 40 ML thick. The fact that the frequency data in Figure 9 shows some curvature suggests that either the stress is less in the thicker Pd films or that relaxation processes come into play. However, much of the deviation from linearity is captured by the uncertainties stated for the two slopes. For example, if $\Delta f_{\text{ML}}^{\text{AT}}$ is determined from only the first three data points (representing Pd films less than 5 ML thick), this will increase the calculated value of the stress to -1.0 GPa , still well below the cantilever-derived stress value but within the stated uncertainties of the EQNB measurement.

Conclusions

The stress induced by electrochemical hydrogen adsorption and absorption in very thin palladium layers electrodeposited onto (111)-textured gold has been examined in 0.1 M H_2SO_4 by the cantilever curvature method and by comparing resonant frequency changes on AT- and BT-cut quartz crystals. A compressive surface stress change of about -0.25 N m^{-1} is measured in the hydrogen adsorption region. Compressive stress for hydrogen adsorption is not predicted from charge distribution models for adsorbate-induced surface stress but is consistent with first-principles calculations in the literature as well as

experimental data for H adsorbed on Pt(111). Cantilever measurements in the hydrogen absorption region are consistent with a maximum atomic H/Pd loading of 0.63 and give a compressive stress-thickness change of -0.45 N m^{-1} per ML of Pd, corresponding to a biaxial stress change of -2.0 GPa . A somewhat lower value of -0.80 GPa for a H/Pd loading of 0.68 was obtained from EQNB data using a double crystal technique. Although we do not fully understand the reason for the discrepancy between the two techniques, these stress values fall well within the range of experimental values reported in the literature for β hydride generated both electrochemically and from the gas phase. Although H absorption causes a volume expansion in unstrained Pd, lattice matching the Pd to establish a tensile stress prior to hydrogen charging reduces the residual compressive stress in the hydride film, possibly imparting mechanical stability to these thin films.

Acknowledgment. The authors gratefully acknowledge Carlos Beauchamp for a variety of technical contributions, Abhishek Motayed for electron-beam evaporating the Au cantilever electrodes, and Stefan Leigh for his statistical analysis of the EQNB data. Certain trade names are mentioned for experimental information only, and in no case does it imply a recommendation or endorsement by the NIST.

References and Notes

- Baldauf, M.; Kolb, D. M. *Electrochim. Acta* **1993**, *38*, 2145.
- Hernandez, F.; Baltruschat, H. *Langmuir* **2006**, *22*, 4877.
- Baldauf, M.; Kolb, D. M. *J. Phys. Chem.* **1996**, *100*, 11375.
- Naohara, H.; Ye, S.; Uosaki, K. *J. Electroanal. Chem.* **2001**, *500*, 435.
- Kibler, L. A.; El-Aziz, A. M.; Kolb, D. M. *J. Mol. Catal. A* **2003**, *199*, 57.
- El-Aziz, A. M.; Kibler, L. A. *J. Electroanal. Chem.* **2002**, *534*, 107.
- Naohara, H.; Ye, S.; Uosaki, K. *Electrochim. Acta* **2000**, *45*, 3305.
- Ruban, A.; Hammer, B.; Stoltze, P.; Skriver, H. L.; Nørskov, J. K. *J. Mol. Catal. A* **1997**, *115*, 421.
- Stafford, G. R.; Bertocci, U. *J. Phys. Chem. C* **2009**, *113*, 261.
- Attard, G. A.; Bannister, A. *J. Electroanal. Chem.* **1991**, *300*, 467.
- Gabrielli, C.; Grand, P. P.; Lasia, A.; Perrot, H. *J. Electrochem. Soc.* **2004**, *151*, A1937.
- Czerwinski, A.; Marassi, R.; Zamponi, S. *J. Electroanal. Chem.* **1991**, *316*, 211.
- Shimazu, K.; Kita, H. *J. Catal.* **1983**, *83*, 407.
- Chevillot, J.-P.; Farcey, J.; Hinnen, C.; Rousseau, A. *J. Electroanal. Chem.* **1975**, *64*, 39.
- Bartlett, P. N.; Gollas, B.; Guerin, S.; Marwan, J. *Phys. Chem. Chem. Phys.* **2002**, *4*, 3835.
- Tateishi, N.; Yahikozawa, K.; Nishimura, K.; Suzuki, M.; Iwanaga, Y.; Watanabe, M.; Enami, E.; Matsuda, Y.; Takasu, Y. *Electrochim. Acta* **1991**, *36*, 1235.
- Cammarata, R. C. *Surf. Sci.* **1992**, *279*, 341.
- Ibach, H. *Surf. Sci. Rep.* **1997**, *29*, 193.
- Haiss, W. *Rep. Prog. Phys.* **2001**, *64*, 591.
- Floro, J. A.; Chason, E.; Commarata, R. C.; Srolovitz, D. J. *MRS Bull.* **2002**, 19–25.
- Floro, J. A.; Hearne, S. J.; Hunter, J. A.; Kotula, P.; Chason, E.; Seel, S. C.; Thompson, C. V. *J. Appl. Phys.* **2001**, *89*, 4886.
- Kongstein, O. E.; Bertocci, U.; Stafford, G. R. *J. Electrochem. Soc.* **2005**, *152*, C116.
- Ibach, H. *J. Vac. Sci. Technol.* **1994**, *A12*, 2240.
- Mickelson, L.; Heaton, T.; Friesen, C. *J. Phys. Chem. C* **2008**, *112*, 1060.
- Trimble, T.; Tang, L.; Vasiljevic, N.; Dimitrov, N.; van Schilfgaarde, M.; Friesen, C.; Thompson, C. V.; Seel, S. C.; Floro, J. A.; Sieradzki, K. *Phys. Rev. Lett.* **2005**, *95*, 166106.
- Vasiljevic, N.; Trimble, T.; Dimitrov, N.; Sieradzki, K. *Langmuir* **2004**, *20*, 6639.
- Viswanath, R. N.; Kramer, D.; Weissmuller, J. *Electrochim. Acta* **2008**, *53*, 2757.
- Feibelman, P. *J. Phys. Rev. B* **1997**, *56*, 2175.
- Cheek, G. T.; O'Grady, W. E. *J. Electroanal. Chem.* **1990**, *277*, 341.
- Gabrielli, C.; Grand, P. P.; Lasia, A.; Perrot, H. *Electrochim. Acta* **2002**, *47*, 2199.
- Grasjo, L.; Seo, M. *J. Electroanal. Chem.* **1990**, *296*, 233.
- Grden, M.; Kotowski, J.; Czerwinski, A.; Solid Stae, J. *Electrochem.* **1999**, *3*, 348.
- Lukaszewski, M.; Czerwinski, A. *J. Electroanal. Chem.* **2006**, *589*, 76.
- Seo, M.; Aomi, M. *J. Electrochem. Soc.* **1992**, *139*, 1087.
- Cermak, J.; Kufudakis, A.; Lewis, F. A. *Z. Phys. Chem.* **1993**, *181*, 233.
- Han, J.-N.; Pyun, S.-I. *Electrochim. Acta* **2000**, *45*, 2781.
- Han, J.-N.; Pyun, S.-I.; Kim, D.-J. *Electrochim. Acta* **1999**, *44*, 1797.
- Sahu, S. N.; Scarminio, J.; Decker, F. *J. Electrochem. Soc.* **1990**, *137*, 1150–1154.
- Okuyama, S.; Mitobe, Y.; Okuyama, K.; Matsushita, K. *Jpn. J. Appl. Phys.* **2000**, *39*, 3584.
- Fabre, A.; Finot, E.; Demoment, J.; Contreras, S. *Ultramicroscopy* **2003**, *97*, 425.
- Hu, Z.; Thundat, T.; Warmack, R. J. *J. Appl. Phys.* **2001**, *90*, 427.
- Huang, X. M. H.; Manolidis, M.; Jun, S. C.; Hone, J. *J. Appl. Phys. Lett.* **2005**, *86*, 143104.
- Yang, F.; Li, J. C. M. *J. Appl. Phys.* **2003**, *93*, 9304.
- Rafizadeh, H. *Phys. Rev. B* **1981**, *23*, 1628.
- EerNisse, E. P. *J. Appl. Phys.* **1972**, *43*, 1330.
- EerNisse, E. P. *J. Appl. Phys.* **1973**, *44*, 4482.
- Stafford, G. R.; Bertocci, U. *J. Phys. Chem. B* **2006**, *110*, 15493.
- Stoney, G. G. *Proc. R. Soc. London Ser. A* **1909**, *82*, 172.
- Kibler, L. A.; Kleinert, M.; Randler, R.; Kolb, D. M. *Surf. Sci.* **1999**, *443*, 19.
- Trasatti, S.; Petrii, O. A. *Pure Appl. Chem.* **1991**, *63*, 711.
- Naohara, H.; Ye, S.; Uosaki, K. *J. Phys. Chem. B* **1998**, *102*, 4366.
- Takahashi, M.; Hayashi, Y.; Mizuki, J.; Tamura, K.; Kondo, T.; Naohara, H.; Uosaki, K. *Surf. Sci.* **2000**, *461*, 213–218.
- Herrero, E.; Buller, L. J.; Abruna, H. *Chem. Rev.* **2001**, *101*, 1897.
- Wilms, M.; Broekmann, P.; Stuhlmann, C.; Wandelt, K. *Surf. Sci.* **1998**, *416*, 121.
- El-Aziz, A. M.; Kibler, L. A.; Kolb, D. M. *Electrochem. Commun.* **2002**, *4*, 535.
- Frumkin, A.; Petrii, O. *Electrochim. Acta* **1975**, *20*, 347.
- Simmons, G. Wang, H. *Single Crystal Elastic Constants and Calculated Aggregate Properties: A Handbook*; M.I.T. Press: Cambridge, MA, 1971.
- Sauerbrey, G. *Z. Phys.* **1959**, *155*, 206.
- Kanazawa, K. K.; Gordon, J. G. *Anal. Chem.* **1985**, *57*, 1770.